Flow driven by a hot wire immersed in a horizontal liquid layer

J.-F. Mercier, C. Normand*

CEA/Saclay, Service de Physique Théorique, F-91191 Gif-sur-Yvette Cedex, France

Abstract

The thermocapillary or buoyancy-driven flow induced by a hot wire placed beneath the free surface of an horizontal liquid layer is determined. The temperature distribution induced by the wire is obtained in a conductive state by the method of images. The upper surface is assumed adiabatic, whereas the lower surface is taken either conductive or adiabatic. Then, the flow driven by the horizontal thermal gradient and the associated deformation of the free surface are determined, considering the action of either thermocapillary or buoyancy effects. In the latter case, a simplified expression of the temperature distribution is used in order to obtain analytical results. Depending on whether thermocapillary or buoyancy effects are considered, the deflection of the free surface above the wire is found to be either concave or convex. © 1998 Elsevier Science Ltd. All rights reserved.

Nomenclature

a height of the fluid layer above which the horizontal temperature distribution is approximated by Θ_S

A aspect ratio, $A = d/L$

b distance between the wire and the bottom boundary in non dimensional unit

b_w distance between the wire and the bottom boundary: $b_w = bd$

Bo Bond number

Ca capillary number

d thickness of the plane horizontal fluid layer

d_w distance between the wire and the top free surface

F, G piecewise-linear profiles of temperature, functions of the y variable: $F(y), G(y)$

F_1, G_1 integrals of $F(y)$ and $G(y)$

g gravity acceleration

h height of the deformed free surface in non dimensional unit

H height of the deformed free surface, function of the x variable: $H(x) = h(x)d$

L horizontal extent of the fluid layer

L_w length of the wire

Ma Marangoni number

p pressure perturbation

P pressure

P_a atmospheric pressure

P_E electrical power

Pr Prandtl number

Q strength of the heat source

r distance from the hot wire

r_c radius of the wire

r_i distance from a sink of heat image of the wire

Ra Rayleigh number

Re Reynolds number

t time

T temperature

T_b bottom boundary temperature

T_c surface temperature of the wire

T_f temperature distribution due to a heat source of strength Q

T_i temperature distribution due to a sink of heat of strength $-Q$

T_1 temperature distribution due to a source and a sink of heat symmetrical with respect of a plane conducting boundary, $T_1 = T_f + T_i$

T_2 temperature distribution due to a source and a sink of heat located at $y = 2 \pm b$

T_w temperature of the lateral walls

u horizontal component of the velocity

U_S characteristic value of the horizontal velocity

* Corresponding author.

v vertical component of the velocity
V_S characteristic value of the vertical velocity
W ratio of Rayleigh number to Marangoni number
x horizontal coordinate
y vertical coordinate
z complex number, $z = x + iy$.

Greek symbols
α thermal expansion coefficient
γ derivative of surface tension with respect to temperature
η dynamical viscosity
θ complex temperature
Θ_S surface temperature distribution
Θ_W horizontal temperature distribution at the wire level
κ thermal diffusivity
λ coefficient in the relationship between Θ_S and Θ_W
μ coefficient in the relationship between h and Θ_S
μ_1, μ_2 coefficients in the expression of the flux conservation condition
v kinematic viscosity
ρ fluid density
σ surface tension
χ thermal conductivity
ψ streamfunction.

1. Introduction

Flows induced by localized heat sources arise in many technological applications and several configurations have already been studied both experimentally and theoretically. In this contribution, we are interested in flows occurring in horizontal liquid layers and driven either by surface tension effects acting on the upper free surface of the fluid layer or by buoyancy effects. In our case, temperature variations are ensured by the presence of a hot wire underneath the free surface. We are primarily concerned with the determination of the temperature distribution in the fluid induced by the wire, the associated flow and the deformation of the free surface above the wire. Our analysis is motivated by recent experimental results obtained when the liquid is placed in rectangular vessels and heated by an electric wire parallel to either the short sides or the long sides of the rectangular horizontal cross-section. We shall refer to a first set of experiments [1, 2] designed to study temporal chaos and where the wire has a short extent. Another experimental team [3, 4] has used a long wire and it was shown that the primary flow undergoes a transition towards unstable modes which were identified as traveling waves propagating along the wire. According to the distance between the wire and the free surface, the spatial properties of these waves vary. When the wire is located at a small distance from the surface, there are two waves traveling in opposite directions while for larger immersion lengths

and near the threshold of instability there is a unique wave traveling from one side to the opposite of the container.

Before understanding the instability mechanism, we shall first focus on the nature of the primary flow. Flows induced by a linear source of heat have received attention in the past mainly when the motion is allowed to develop in infinite or semi-infinite medium. This has led to the theory of plumes where progress in the knowledge of these systems resulted from similarity analyses [5]. Much less is known when the flow is confined between horizontal boundaries where former results obtained in this geometry considered a source of heat external to the fluid. The analysis of Pimputkar and Ostrach [6] for transient thermocapillary flow is based on a thin liquid layer approximation. Numerical results were obtained by these authors for a fixed Gaussian surface temperature distribution. Later on, Hitt and Smith [7] emphasize on the constant change in the free-surface temperature as the height of liquid thins and they have included this coupling when considering radiation-driven thermocapillary flows, the radiative heating being induced by an external infinite cylindrical heater located above the free surface. Despite some similarities with the thermocapillary flows considered in Refs 6 and 7, our motivations are different and in particular we are not concerned with strong interfacial deformations that can lead to the breaking of the liquid layers as allowed in Refs 6 and 7. In our model, the deformations are small enough for the hot wire to always be submerged in the liquid. Moreover, one cannot exclude that under the experimental conditions reported in Refs 3 and 4, the flow is driven by buoyancy as well as by thermocapillarity since the height of fluid above the wire can be varied, ranging from 1–4 mm, while the height of fluid below the wire is fixed and equal to 10 mm. The particular configuration corresponding to heating from a line source of heat located on the bottom plate was never reached in Refs 3 and 4, contrary to what happens in other experiments [8, 9] specially devoted to this geometry. In these latter cases the flow is constituted of an ascending buoyant plume which is deflected horizontally by the free surface and the interfacial deformations result in a straight bump above the heat source. On the contrary, when thermocapillary effects are dominant, the fluid is drawn away from the hot regions which result in a depression of the interface in these regions.

2. Formulation

Consider an infinite horizontal liquid layer, that is initially at the uniform thickness d. The fluid is bounded below by a rigid, isothermal plate maintained at temperature T_b, and above by a thermally insulated free surface. It is assumed that the physical properties of the fluid such as kinematic viscosity v, thermal conductivity

χ and diffusivity κ are constant and until Section 5 the density ρ is also assumed constant. The liquid free surface has a surface tension σ whose variations are due to a linear dependence on temperature

$$\sigma = \sigma_0 - \gamma(T - T_b)$$

where $\gamma = -d\sigma/dT$ is positive and σ_0 is a reference value. The liquid is subjected to Joule heating from an electric wire immersed horizontally in the fluid at a height, $b_w = bd$ ($0 < b < 1$), from the bottom plate as shown in Fig. 1. If the radius of the wire is assumed small compared to the height b_w, it can be imagined that the temperature and heat flow around it are produced by a line source of heat of strength Q, located on the centre of the wire, creating at a distance r a thermal gradient $(\partial T/\partial r) = -(Q/2\pi\chi r)$. Assuming an infinite extent of the wire along the direction perpendicular to the (Ox, Oy) plane, it is expected that temperature gradients will give rise to a two-dimensional fluid motion in the (Ox, Oy) plane, governed by the equations

$$\partial_x u + \partial_y v = 0 \tag{1a}$$

$$\partial_t u + u\,\partial_x u + v\,\partial_y u = -\frac{1}{\rho}\partial_x P + \nu(\partial_{xx}u + \partial_{yy}u) \tag{1b}$$

$$\partial_t v + u\,\partial_x v + v\partial_y v = -\frac{1}{\rho}\partial_y P + \nu(\partial_{xx}v + \partial_{yy}v) - g \tag{1c}$$

$$\partial_t T + u\,\partial_x T + v\,\partial_y T = \kappa(\partial_{xx}T + \partial_{yy}T) \tag{1d}$$

where u and v are the velocity components in x and y, and P is the pressure. The boundary conditions are on the bottom plate

$$u = v = 0, \quad T = 0 \quad \text{at } y = 0$$

and on the slightly deformed free surface assumed at rest

$$\left.\begin{array}{ll} v = u\,\partial_x H & 2\eta\,\partial_y v - P = \sigma\,\partial_{xx}H - P_a \\ \eta\,\partial_y u = -\gamma\,\partial_x T & \partial_y T = \partial_x T\,\partial_x H \end{array}\right\} \text{at } y = H(x),$$

$$H(x) \to d \quad \text{when } x \to \pm\infty$$

with $\eta = \nu\rho$, being the dynamical viscosity and P_a the atmospheric pressure.

The temperatures being scaled with $Q/2\pi\chi$ and the lengths with d, it comes from the balance of tangential stress that the characteristic value of the velocity in our problem is

$$\bar{U}_s = \frac{\gamma}{\eta}\frac{Q}{2\pi\chi}.$$

Thus, in non dimensional form, equation (1d) can be rewritten

$$Ma(\partial_t T + u\,\partial_x T + v\,\partial_y T) = \partial_{xx}T + \partial_{yy}T$$

with the Marangoni number defined as

$$Ma = \frac{\bar{U}_s d}{\kappa}.$$

The fluid used in the experiments that have motivated this study is a silicon oil having a Prandtl number $Pr = 135$, the numerical values of its physical properties can be found in Ref. 2. In the experiments reported in Ref. 3 the length of the wire is $L_w = 60$ cm and the control parameter is the electrical power P_E, which is related to Q by $P_E = QL_w$. Thus, an estimation of the experimental Marangoni number leads to $Ma^{ex} = 100P_E d$ where P_E, is expressed in Watts and d, the distance is expressed in millimeter. The value of P_E never exceeds 12 W to avoid deformation of the wire and boiling of the silicon oil. It appears that the experimental results are not very sensitive to the total height of fluid d, but rather strongly depend on the distance between the wire and the free surface that ranges from $d_w = 0.8$–4 mm. When thermocapillary effects are dominant, that is for $d_w < 2$ mm, it has been shown in Ref. 3 that the primary flow remains stable for values of $P_E d_w < 4$ W mm. Thus, at the threshold of instability the convective terms in equation (1d) cannot be neglected, and once the threshold is
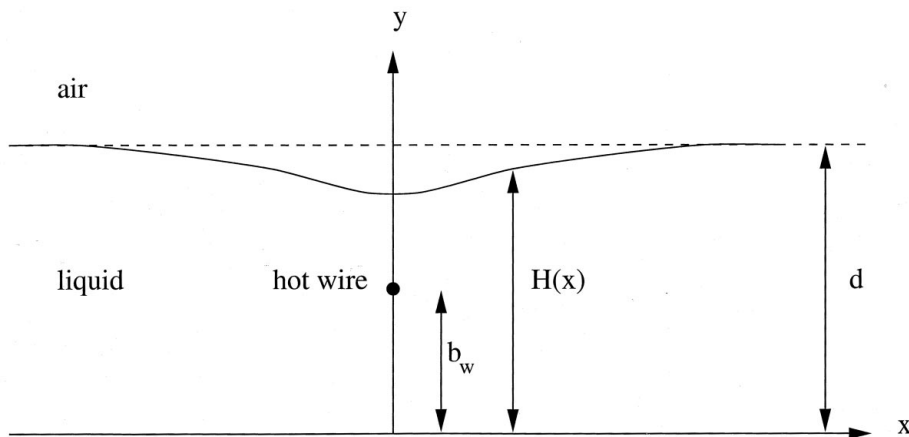

Fig. 1. Geometry of the problem.

exceeded they become more and more important so that the diffusive terms can be neglected and the temperature ultimately evolves through the advection equation

$$\partial_t T + u\,\partial_x T + v\,\partial_y T = 0.$$

This assumption, together with a low value of the Reynolds number, has been used recently to derive a two-dimensional model for thermal or solutal Marangoni convection [10]. According to this approach, the velocity field is derived from the Stokes equation and only depends on the initial surface temperature distribution that is supposed to be known. Different temperature fields have been considered, the simpler cases being represented by Dirac or trigonometric function. In the present case, the temperature distribution due to the hot wire is not known and has first to be determined. This will be done assuming the fluid is at rest with the temperature variations in both the x and the y directions satisfying the conduction equation

$$\partial_{xx} T + \partial_{yy} T = 0.$$

This approach that consists in determining the temperature distribution in the conductive regime and then the flow induced by thermal gradients has already been used by Yu and Nansteel [11] who addressed the problem of buoyancy-induced Stokes flow in a sectorial region.

In the next section, after assuming a plane interface at $y = d$, we shall determine the temperature distribution due to the hot wire as if the fluid was at rest. Then, in Section 4 we shall deduce the velocity field and the interfacial deformations when only thermocapillary effects are taken into account. In Section 5, we will show how the present formulation must be modified to describe the flow driven by buoyancy effects. Finally, the coupling of buoyancy and thermocapillarity will be considered in Section 6.

3. Temperature distribution

Let us first recall that if a wire of radius r_c is embedded in an infinite medium, the temperature distribution at a distance, r, from the centre of the wire would be [12]

$$T_f = T_c - \frac{Q}{2\pi\chi}\ln\frac{r}{r_c}, \tag{2}$$

where Q is the Joulean heat released per unit length of the wire, and T_c is the wire surface temperature. The next step in view of obtaining the temperature distribution created by a line source of heat embedded in a medium confined between two horizontal boundaries, is to consider a semi-infinite medium bounded at $y = 0$ by an isothermal surface maintained at the temperature T_b. The wire being located at $y = b_w$, the problem is solved by the method of images which consists in supposing an image of the wire to exist, symmetrical to the plane $y = 0$. The

image located at $y = -b_w$ is a sink of heat, of strength $-Q$ and of surface temperature $-T_c$.

Corresponding to equation (2), the temperature distribution produced by the sink at a distance, r_i, from its centre is

$$T_i = -T_c + \frac{Q}{2\pi\chi}\ln\frac{r_i}{r_c}. \tag{3}$$

The temperature distribution at a point of coordinates (x, y) is the superposition of the two contributions (2) and (3)

$$T = T_f + T_i = \frac{Q}{2\pi\chi}\ln\frac{r_i}{r} \tag{4}$$

where

$$r^2 = x^2 + (y-b)^2 \quad \text{and} \quad r_i^2 = x^2 + (y+b)^2$$

are now non dimensional variables, the lengths being scaled with d. Substitution of the above expressions into equation (4) yields

$$T \equiv T_1 = \frac{Q}{4\pi\chi}\ln\frac{x^2+(y+b)^2}{x^2+(y-b)^2} \tag{5}$$

where T_1 represents the excess temperature over the fixed bottom temperature T_b.

The formula (5) is no longer true when a thermally insulated top boundary is present in the system at $y = 1$. To satisfy the prescribed top boundary condition $\partial T/\partial y = 0$, one can once again apply the method of images and consider images, symmetrical to the plane $y = 1$, of the source at $y = b$ and of the sink at $y = -b$. Their images are respectively a source of heat located at $y = 2-b$ and a sink at $y = 2+b$. Taking into account this couple of source and sink leads to a new contribution for the temperature

$$T_2 = \frac{Q}{4\eta\chi}\ln\frac{x^2+(y-2-b)^2}{x^2+(y-2+b)^2}. \tag{6}$$

Superposition of the formulas (5) and (6) yields an expression for the temperature distribution

$$T \equiv T_1 + T_2$$

which allows satisfaction of $\partial T/\partial y = 0$, at $y = 1$, but not $T = 0$ at $y = 0$. Therefore, to satisfy simultaneously the thermal boundary conditions on the top and bottom plates it is necessary to introduce an infinite number of sources and sinks which are distributed by doing alternately an antisymmetry with respect to the plane $y = 0$, and a symmetry with respect to the plane $y = 1$. This gives rise to an infinite row of sources and sinks located, respectively, at

$$y = b, \quad \pm 2-b, \quad \pm 4+b, \ldots, \pm 2n+(-1)^n b, \ldots$$

for the sources of strength Q

and

$$y = -b, \quad \pm 2 + b, \quad \pm 4 - b, \ldots, \pm 2n - (-1)^n b, \ldots$$

$$\text{for the sinks of strength } -Q.$$

To derive the temperature distribution due to this infinite row of sources and sinks it is convenient to introduce the complex variable $z = x + iy$ and the function $\theta(z) = T + i\bar{T}$.

Expression (5) for T is recovered by taking the real part of

$$\theta(z) = -\frac{Q}{2\pi\chi}[\ln(z - ib) - \ln(z + ib)]. \tag{7}$$

Generalization to the infinite row of sources and sinks we are considering, yields

$$\theta(z) = -\frac{Q}{2\pi\chi} \sum_{n=0}^{\infty} \ln\{z - i[\pm 2n + (-1)^n]\}$$

$$- \ln\{z - i[\pm 2n - (-1)^n b]\}.$$

Summation of the series is obtained after derivation of the above expression in which we recognize the expansion [13]

$$\frac{\text{ch}\, k\pi/2}{\text{sh}\, k\pi} = \frac{1}{\pi}\left(\frac{1}{k} - \frac{2k}{2^2 - k^2} + \frac{2k}{4^2 + k^2} - \frac{2k}{6^2 + k^2} + \cdots\right)$$

that appears a first time with $k = z - ib$, and the second time with $k = z + ib$. Thus

$$\frac{d\theta}{dz} = -\frac{Q}{2\chi}\left(\frac{\text{ch}(z - ib)\pi/2}{\text{sh}(z - ib)\pi} - \frac{\text{ch}(z + ib)\pi/2}{\text{sh}(z + ib)\pi}\right)$$

and

$$\theta(z) = -\frac{Q}{2\pi\chi}\ln\left(\frac{\text{th}(z - ib)\pi/4}{\text{th}(z + ib)\pi/4}\right). \tag{8}$$

The temperature distribution $T(x, y)$ is the real part of the above expression. The isothermal lines have been drawn in Fig. 2 for three different values of b.

Since we are interested in thermocapillary-driven flow, we are mainly concerned with the horizontal variations of temperature, $\partial T/\partial x$, at the interface $y = 1$. It comes from the definition of θ that $\partial T/\partial x$ is identical to the real part of $d\theta/dz$ which expresses as

$$\frac{\partial T}{\partial x} = -\frac{Q}{2\chi}\text{sh}\frac{\pi x}{2}\left(\frac{\cos(y - b)\pi/2}{\text{ch}\,\pi x - \cos\pi(y - b)}\right.$$

$$\left. - \frac{\cos(y + b)\pi/2}{\text{ch}\,\pi x - \cos\pi(y + b)}\right). \tag{9}$$

The corresponding isogradient lines are drawn in Fig. 3. When evaluated at $y = 1$, the above expression reduces to

$$\left.\frac{\partial T}{\partial x}\right|_1 = -\frac{Q}{\chi}\sin\frac{\pi b}{2}\,\text{sh}\frac{\pi x}{2}\frac{1}{\text{ch}\,\pi x + \cos\pi b}, \tag{10}$$

showing that far from the wire, at large absolute values of x, the horizontal gradient decays exponentially like

$\exp(-\pi|x|2)$. But due to the factor $\sin(\pi b/2)$, the asymptotic decay is less pronounced when the wire is close to the interface ($b \to 1$). The variations of $\partial_x T|_1$ are plotted in Fig. 4 for different positions of the wire. It is shown that the horizontal thermal gradient reaches a maximum value at a distance x_0 that is roughly equal to $1 - b$. The maximum absolute value of $\partial_x T|_1$ proportional to tg $(\pi b/2)$ tends to infinity as $b \to 1$, its value being multiplied by a factor 10 when b goes from 0.2–0.8. At a distance $x = 2d$ the value of $\partial_x T|_1$ for $b = 0.8$ is three time larger than its value for $b = 0.2$.

The asymptotic behavior of $\partial T/\partial x$ could be quite different with a different choice of thermal boundary condition on the bottom plate. For instance, if the bottom plate is insulated, the method of images generates an infinite row of sources of equal strength Q, and the problem of finding $\theta(z)$ becomes identical to that of finding the potential- and stream-functions due to an infinite row of co-rotating vortices in hydrodynamics. The solution is known for equidistant sources [13] as well as in the general case [14] and leads to

$$\frac{d\theta}{dz} = -\frac{Q}{2\chi}\left(\frac{\text{sh}\,\pi z}{\text{ch}\,\pi z - \cos\pi b}\right).$$

When the wire is located at mid-height ($b = 1/2$) the horizontal thermal gradient takes a simple form

$$\frac{\partial T}{\partial x} = -\frac{Q}{2\chi}\left(\frac{\text{sh}\,2\pi x}{\text{ch}\,2\pi x + \cos 2\pi y}\right) \tag{11}$$

and tends towards a constant value as $x \to \pm\infty$. Therefore, at some distance from the wire, the temperature becomes independent of the vertical coordinate y. When the bottom boundary is insulating, its temperature T_b is not controlled and cannot be used as a temperature reference. As in many experimental situations, the fixed temperature is T_w the temperature of the lateral walls that confined the fluid at $x = \pm L/d$. Integration of equation (11) leads to

$$T = T_w - \frac{Q}{4\pi\chi}\ln\left(\frac{\text{ch}\,2\pi x + \cos 2\pi y}{\text{ch}\,2\pi L/d + \cos 2\pi y}\right).$$

In the limit $L \to \infty$, the corresponding isothermal lines $T - T(0, 1)$ and the lines of isogradient are drawn in Figs 5 and 6 when the wire is located at mid-height and the bottom plate is insulating.

4. Thermocapillary-driven flow

The temperature distribution found in the previous section creates a steady flow that causes deformation of the free surface which is now located at $y = H(x) = h(x)d$. We shall assume that surface tension effects are predominant when the wire is located near the free surface. When restricted to this configuration, it has been shown in the previous section that the horizontal vari-
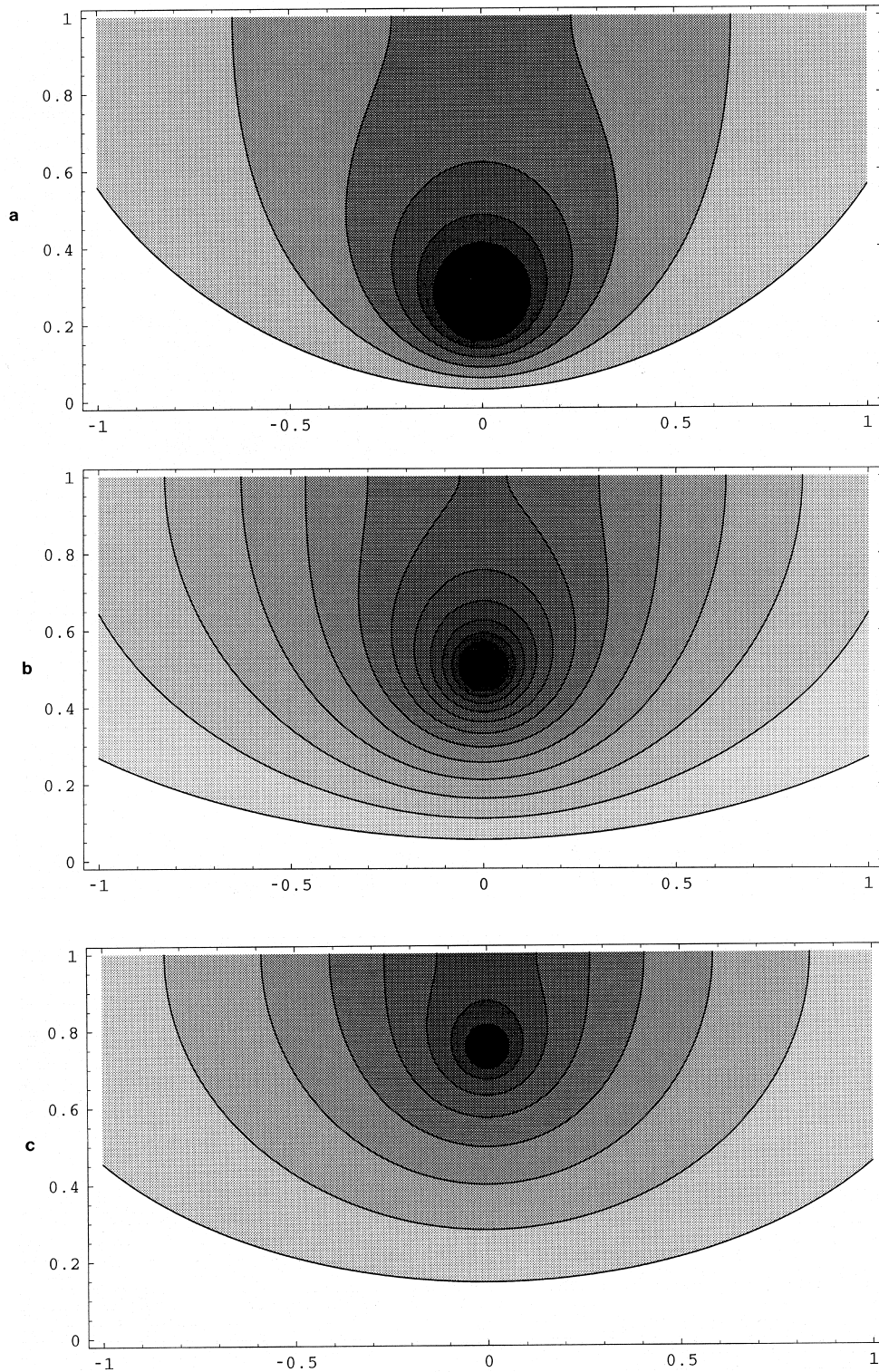
Fig. 2. Isothermal lines $T - T_b$ in $Q/4\pi\chi$ units for different positions, $y = b$, of the wire, in the case of an adiabatic upper surface and a conducting lower surface. Dark areas correspond to hot fluid: (a) $b = 0.25$, isovalues between 0 and 1.75 with step size 0.25; (b) $b = 0.5$, isovalues between 0 and 4 with step size 0.25; (c) $b = 0.75$, isovalues between 0 and 4 with step size 0.5.
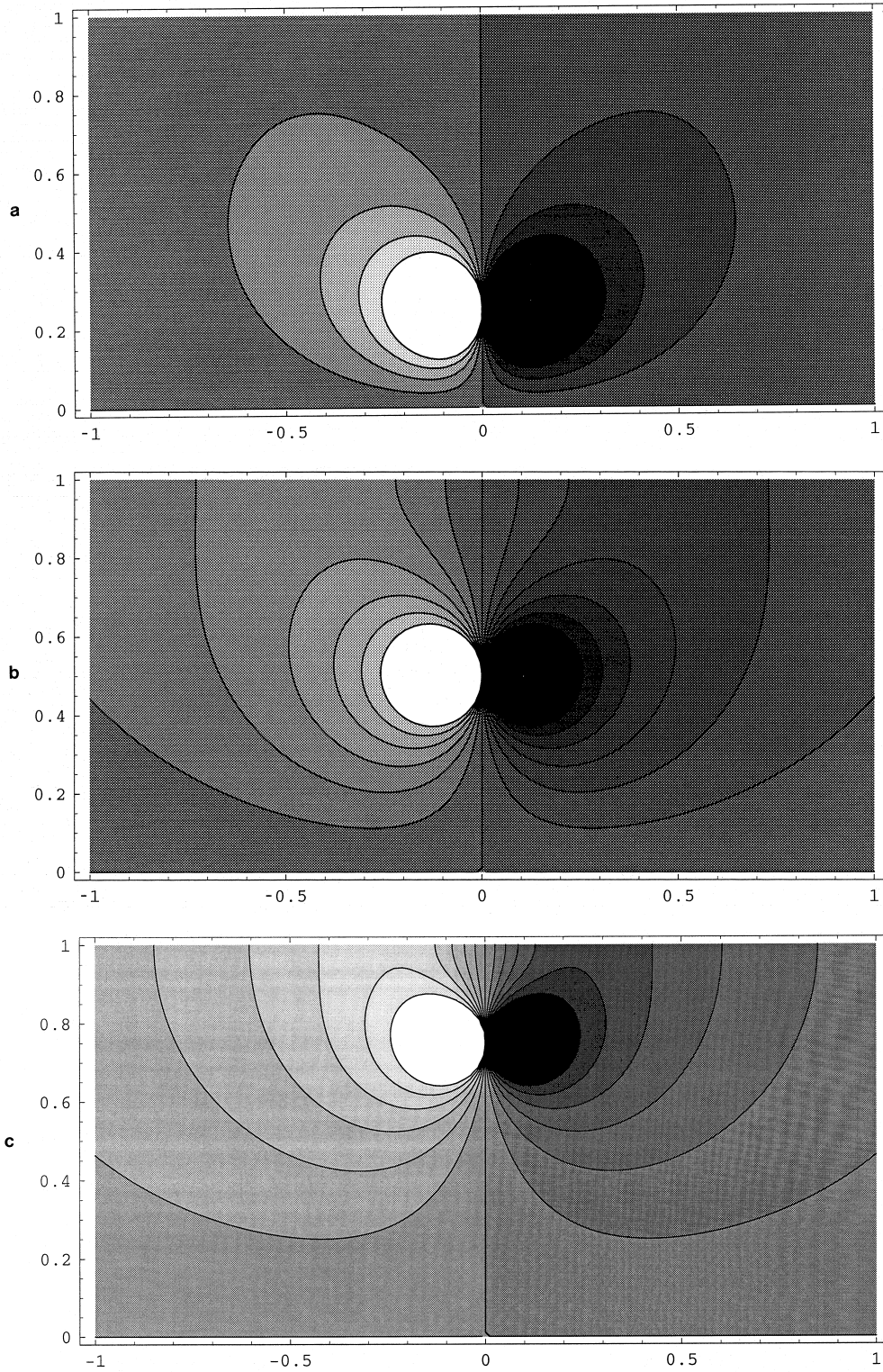
Fig. 3. Isogradient lines of temperature in the *x*-direction for different positions, $y = b$, of the wire, in the case of adiabatic-conducting thermal boundaries conditions: (a) $b = 0.25$, isovalues between -1 and 1 with step size 0.25; $b = 0.5$, isovalues between -1.2 and 1.2 with step size 0.2; (c) $b = 0.75$, isovalues between -1.5 and 1.5 with step size 0.25.
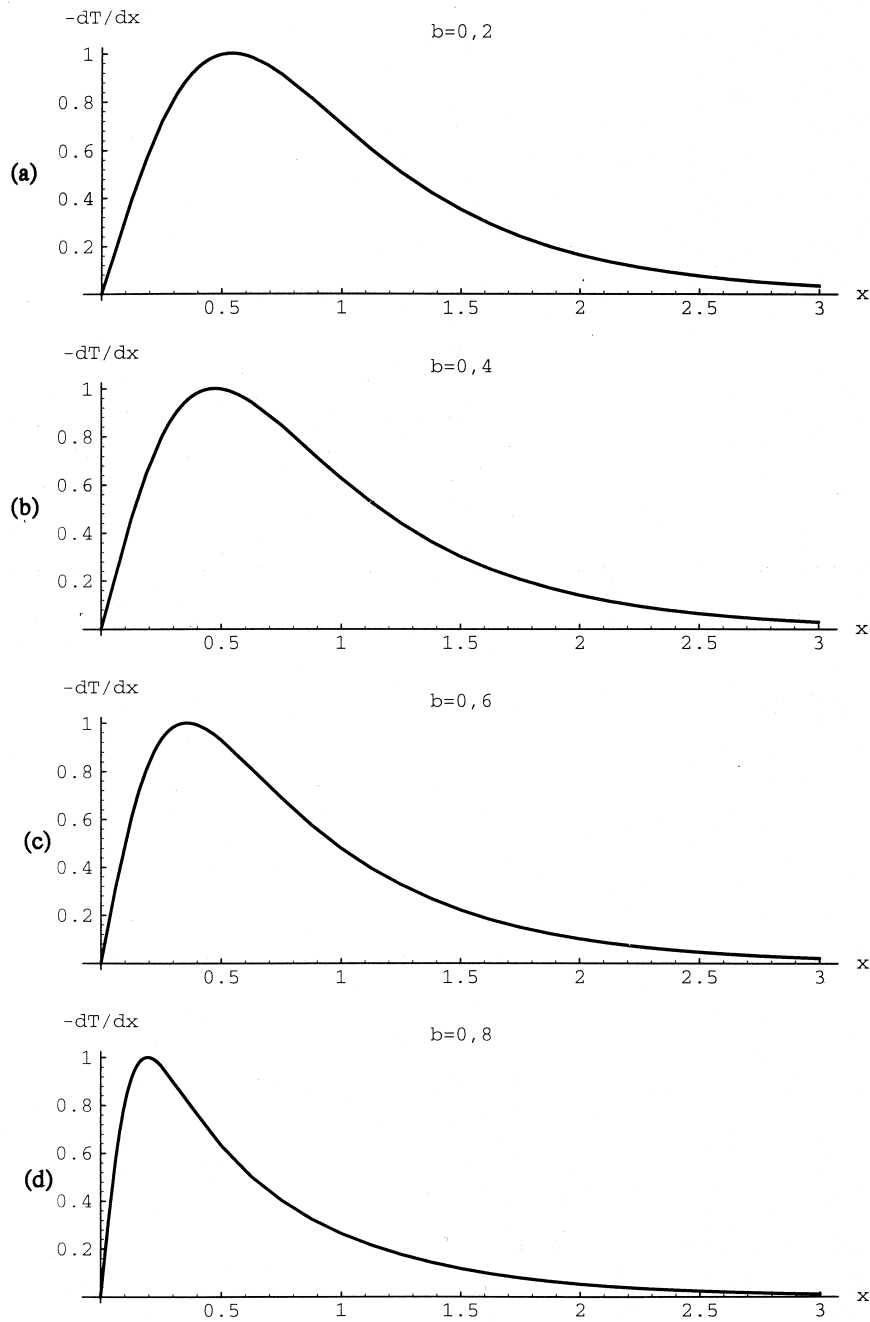
Fig. 4. Absolute value of the horizontal gradient of temperature on the free surface [normalized to unity after division by the factor tg($\pi b/2$)] for different positions of the wire: (a) $b = 0.2$, tg($\pi b/2$) = 0.325; (b) $b = 0.4$, tg($\pi b/2$) = 0.726; (c) $b = 0.6$, tg($\pi b/2$) = 1.376; (d) $b = 0.8$, tg($\pi b/2$) = 3.077.

ations of the temperature evolve over distances that exceed the thickness of fluid at rest. Thus, following the analysis of Pimputkar and Ostrach [5] we have introduced a distinct characteristic length scale, $L \gg d$, in the *x* direction. When the bottom boundary is conducting, *L* measures the extent of the horizontal thermal gradient. When the bottom boundary is insulating, *L* is the distance between the wire and the side walls and it can be taken arbitrarily large. In expression (10) the non dimensional *x*-variable is stretched by the transformation
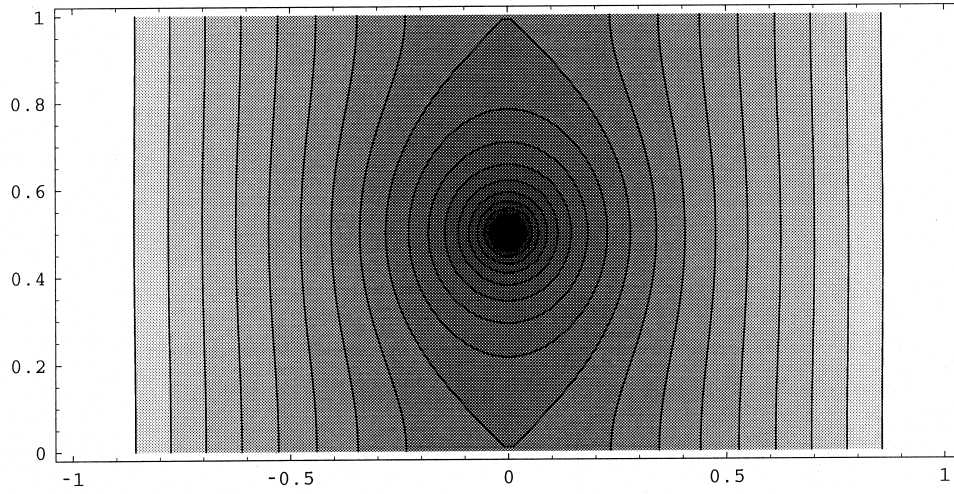
Fig. 5. Isothermal lines $T(x, y) - T(0, 1)$ in $Q/4\pi\chi$ units in the case of adiabatic lower and upper surfaces, with the wire located at mid-height. Isovalues between -2 and 2 with step size 0.25.
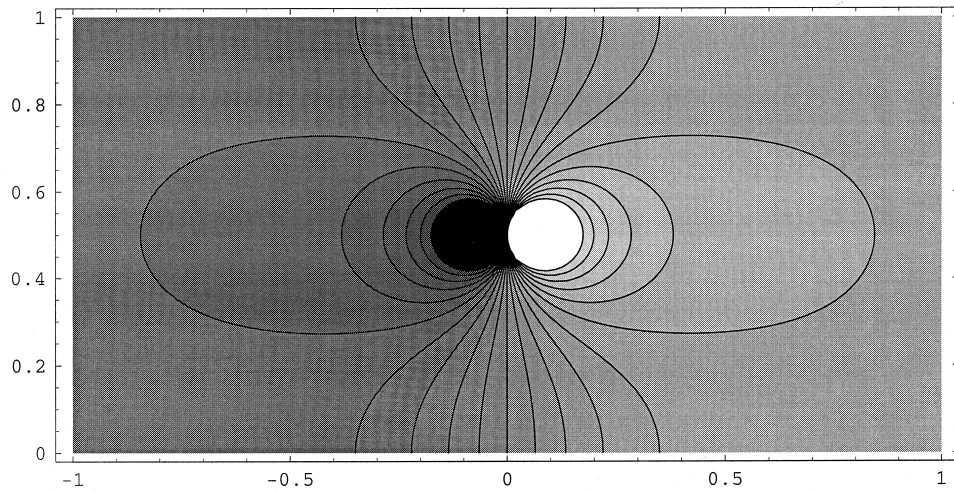

Fig. 6. Isogradient lines of temperature in the x-direction in the case of adiabatic lower and upper surfaces, with the wire located at mid-height. Isovalues between -2 and 2 with step size 0.2.

$$x \rightarrow A^{-1}x$$

where $A = d/L$, is the aspect ratio. Therefore, the characteristic value of the horizontal velocity component is now $U_S = A\bar{U}_S$. As a consequence of equation (1a), the characteristic value of the vertical component of the velocity is $V_S = A U_S$. The pressure is decomposed in two contributions

$$P = P_a - \rho g d(y - h) + \frac{\eta U_S L}{d^2} p \qquad (12)$$

where P_a is the atmospheric pressure at $y = h(x)$. Equations (1a)–(1c) become

$$\partial_x u + \partial_y v = 0 \qquad (13a)$$

$$Re\, A^2 (u\,\partial_x u + v\,\partial_y u) = -\partial_x p - Bo\, A\partial_x h + (\partial_{yy} u + A^2 \partial_{xx} u) \qquad (13b)$$

$$Re\, A^4 (u\,\partial_x v + v\,\partial_y v) = -\partial_y p + A^2 (\partial_{yy} v + A^2 \partial_{xx} v) \qquad (13c)$$

with the Reynolds number Re, and Bond number Bo, defined as

$$Re = \frac{\bar{U}_S d}{\nu} \quad \text{and} \quad Bo = \frac{\rho g d^2}{\eta U_S}.$$

We shall notice that the Bond number is sometimes

denoted as the Galileo number. The Reynolds number also expresses as $Re = Ma/Pr$ and with the values of Ma and Pr given in the previous section it comes that $Re < 1$ below the threshold for instability. Thus, either Stokes approximation or thin-layer-approximation can be used to neglect the non linear terms in equations (13b)–(13c). The boundary conditions for the pressure and velocity fields are

$$u = v = 0 \quad \text{at } y = 0$$

$$\left.\begin{array}{l} \partial_y u + \partial_x \Theta = 0 \\ 2A^2\, \partial_y v - p = Ca^{-1}A^3\, \partial_{xx}h \\ v = u\, \partial_x h \end{array}\right\} \quad \text{at } y = h. \quad (14)$$

with the capillary number: $Ca = \eta U_S/\sigma$ and where the surface temperature $\Theta = T(x, h)$ has been introduced. It is assumed that as $A \to 0$, the parameters $Re\,A$ and A^3/Ca also tend to zero while $Bo\,A$ remains fixed.

The pressure is found by solving $\partial_y p = 0$, with $p = 0$ at $y = h$, from which it results that $p(x, y) = 0$. Then, the lowest order of equation (13b) yields

$$\partial_{yy}u = Bo\,A\, \partial_x h \quad (15)$$

with the boundary conditions

$$u = 0 \quad \text{at } y = 0 \quad \text{and} \quad \partial_y u + \partial_x \Theta = 0 \quad \text{at } y = h. \quad (16)$$

The solution of equations (15) and (16) is

$$u = Bo\,A\, \partial_x h \left(\frac{y^2}{2} - yh\right) - y\, \partial_x \Theta.$$

Introducing the streamfunction ψ such that

$$u = \partial_y \psi \quad \text{and} \quad v = -\partial_x \psi$$

we find that

$$\psi = Bo\,A\, \partial_x h \left(\frac{y^3}{6} - \frac{y^2}{2}h\right) - \frac{y^2}{2}\partial_x \Theta$$

and

$$v = -Bo\,A\, \partial_{xx}h \left(\frac{y^3}{6} - \frac{y^2}{2}h\right) + Bo\,A(\partial_x h)^2 \frac{y^2}{2} + \frac{y^2}{2}\partial_{xx}\Theta.$$

Satisfaction of $v = u\, \partial_x h$ at $y = h$, provides the following relation between $h(x)$ and $\Theta(x)$:

$$\partial_x \left(\frac{Bo\,A}{12}\partial_x h^4 + \frac{h^2}{2}\partial_x \Theta\right) = 0.$$

Since $\partial_x h = \partial_x T = 0$ at $x = 0$ and $h = 1$ at $x = \pm\infty$, this can be integrated to give

$$h^2 = 1 - \frac{3\Theta}{Bo\,A} \quad (17)$$

a result originally due to Pimputkar and Ostrach [5] and that is applied in the present case when Θ is specified by either

$$\Theta = -\frac{1}{2\pi}\ln\left(\frac{\text{ch}(\pi x/2A) - \sin(\pi b/2)}{\text{ch}(\pi x/2A) + \sin(\pi b/2)}\right) \quad (18a)$$

when the bottom plate is conducting, or by

$$\Theta = -\frac{1}{2\pi}\ln\left(\frac{\text{ch}\,\pi x/A + \cos\pi b}{\text{ch}\,\pi/A + \cos\pi b}\right) \quad (18b)$$

when the bottom plate is adiabatic.

In the conducting case, the streamfunction given by

$$\psi = -\partial_x \Theta \frac{y^2}{4}\left(\frac{y}{h} - 1\right).$$

and the deformation are shown in Fig. 7 for $b = 3/4$ and two different values of $Bo\,A$. The height of fluid at $x = 0$ is plotted in Fig. 8 as a function of $Bo\,A$. This picture indicates that for $Bo\,A > 20$ the interfacial deformations are weak.

From the experimental data of Ref. 4 we obtain that the variation range of $Bo\,A$ is between 100 and 800. Applying the formulas (17) and (18a) when $Bo\,A = 100$ and $b = 3/4$, we found that the deflection above the wire is of order $10^{-3}d$. Comparison with experiments is difficult since in Ref. 4, interfacial deformations associated to the primary flow have only been observed through shadowgraphic images of the wire but their amplitudes have not been measured.

5. Buoyancy-driven flow

When the distance between the wire and the free surface exceeds 2.5 mm, it has been reported in Ref. 3 that larger values of the electrical power are required to destabilize the base flow. Moreover, the instability pattern consists in disordered propagating waves whereas for lower values of d_W the waves have a well defined wavelength. The authors argue that in that case buoyancy is the predominant mechanism acting in the fluid, thus we shall now examine what has changed in the base state that could explain the different behaviors of the system according to the values of d_W.

We shall consider in this section a fluid with a constant surface tension σ_0, but with a density varying with the temperature according to the law

$$\rho = \rho_0(1 - \alpha(T - T_0))$$

where T_0 is a reference temperature, for instance that of the bottom plate, and α is the coefficient of thermal expansion. Thus, equation (1c) in the governing equations for the steady velocity is replaced by

$$u\, \partial_x v + v\, \partial_y v = -\frac{1}{\rho}\partial_y P + \nu(\partial_{xx}v + \partial_{yy}v) - g(1 - \alpha T)$$

where T is the temperature distribution in the fluid due to the wire. Using the same scaling as in the previous
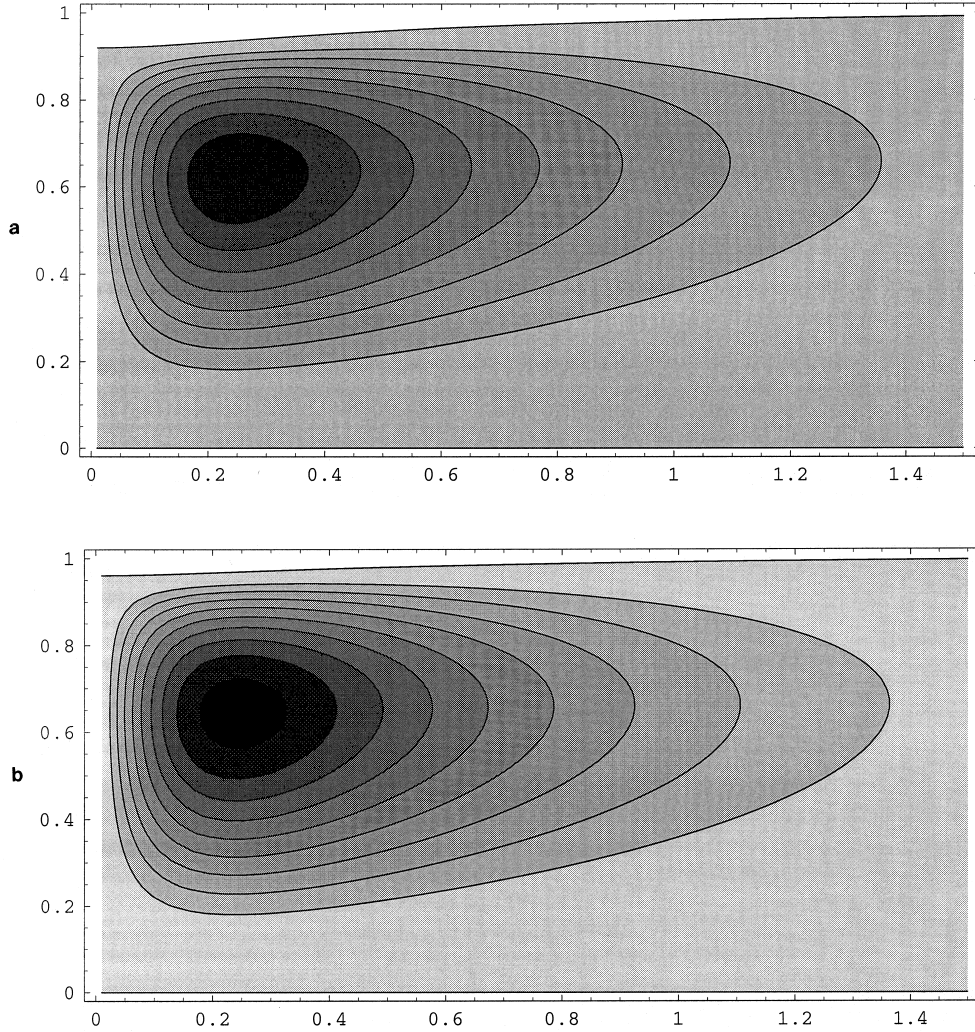
Fig. 7. Streamlines $\psi(x, y)$ and associated deformation of the free surface $h(x)$ in the case of a thermocapillary-driven flow, with the wire located at $b = 0.75$, for two values of the Bond number: (a) $Bo\, A = 10.$; (b) $Bo\, A = 20$. Isovalues between 0. and -0.02 with step size 0.002.

section and with the decomposition of the pressure, equation (12), still valid, it becomes

$$Re\, A^4 (u\, \partial_x v + v\, \partial_y v) = -\, \partial_y p + \frac{\alpha g Q d^3}{v \chi L U_s} T$$
$$+ A^2 (\partial_{yy} v + A^2\, \partial_{xx} v). \quad (19)$$

The combination of parameters that appears in front of T can be set equal to one by the following choice of the characteristic value of the velocity

$$U_s = \frac{\alpha g Q d^3}{v \chi L}.$$

When considering the equation (1d) for heat transfer it

comes from this scaling that the convective terms are of the order $Ra\, A^2$, with the Rayleigh number defined by

$$Ra = \frac{\alpha g Q d^3}{v \chi \kappa}.$$

Under the experimental conditions of Ref. 4, its value can be estimated to $Ra = 30 P_E d^3$, where d is expressed in millimeters.

At the leading order equation (19) reduces to

$$\partial_y p = T(x, y) \quad (20)$$

and the associated boundary condition deduced from equation (14) is: $p = 0$ at $y = h$. It exists a non zero
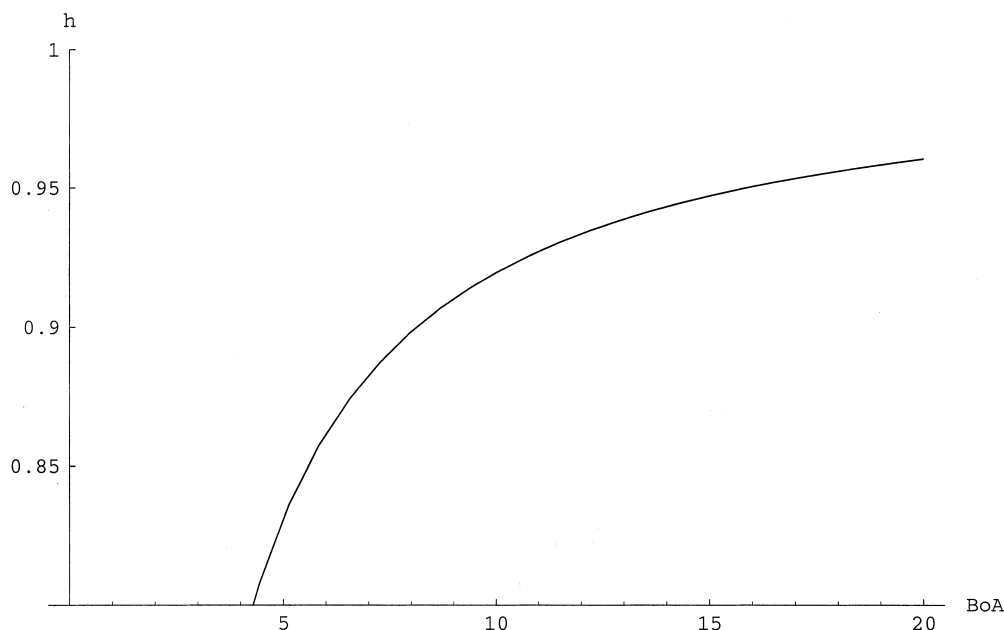
Fig. 8. Height of fluid at $x = 0$, vs *Bo A*. The bottom plate is conducting and $b = 3/4$.

solution for the pressure that is substituted in equation (13b) to give at the leading order

$$\partial_{yy}u = Bo\,A\,\partial_x h + \partial_x p. \tag{21}$$

Since the velocity scale is related to buoyancy, the Bond number now expresses as $Bo\,A = \chi/\alpha Q$. Integration of equation (21) when considering the general expression for $T(x, y)$ will lead to intricate calculations. Examination of Figs 2, 3 and 6 shows that large temperature gradients exist around the wire and we shall now focus on the vertical temperature profile at different values of x.

When the bottom boundary is conducting, it is shown in Fig. 9 that the vertical dependence can be approximated by a piecewise-linear profile in three parts. In the upper part ($a < y < h$) the temperature is assumed to be constant and equal to the surface temperature $\Theta_S(x) = T(x, h)$. In the lower part the temperature increases from zero and reaches a maximum value $\Theta_W(x) = T(x, b)$ at the wire location. An intermediate region ($b < y < a$) allows for the linear matching between Θ_S and Θ_W. As the horizontal distance from the wire increases, the difference between Θ_x and Θ_W reduces and a vertical profile in two parts can be used (Fig. 9(b)).

When the bottom boundary is insulating, the exact vertical temperature distribution and the approximated linear profile are displayed for comparison in Fig. 10 for $x = 0.2$. In this case the value of the temperature on the bottom plate is also of some importance, especially when $x \to 0$. However, when b is small, the maximum gradients are always located between the wire and the free surface. Since we want to capture the essential feature of the

problem we still use a description in terms of two characteristic temperatures Θ_S and Θ_W which is particularly suitable when $x > 1$. Indeed, at large values of x, Θ_S and Θ_W nearly coincide and a flat vertical profile can be used.

The above considerations suggest that the temperature distribution in the fluid can be represented by the superposition of two terms

$$T(x, y) = \Theta_S(x)F(y) + \Theta_W(x)G(y). \tag{22}$$

The vertical temperature distributions $F(y)$ and $G(y)$ are piecewise-linear profiles and $G(y)$ need to be specified for each type of thermal condition on the bottom boundary:

$$F(y) = \begin{cases} 1 & \text{when } a < y < h \\ \dfrac{y-b}{a-b} & \text{when } b < y < a \\ 0 & \text{when } 0 < y < b \end{cases}$$

$$G(y) = \begin{cases} 0 & \text{when } a < y < h \\ \dfrac{a-y}{a-b} & \text{when } b < y < a \\ \dfrac{y}{b} & \text{conducting or 1 (insulating)} \\ & \qquad \text{when } 0 < y < b. \end{cases}$$

The choice of piecewise-linear profiles has been made in the past to describe penetrative convection. As mentioned by Whitehead and Chen [15] this is the simplest temperature distribution to be considered when heat sources are concentrated in the vicinity of a particular depth.

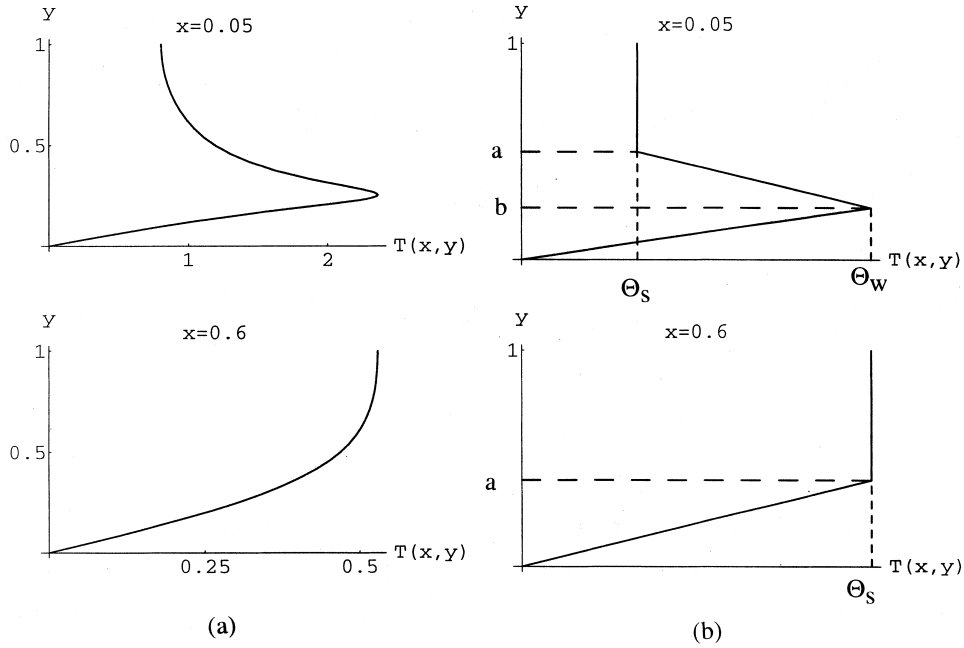Integration of equation (20) yields for the pressure

Fig. 9. Vertical temperature profiles when the bottom plate is conducting and $b = 0.25$. (a) exact profiles for $x = 0.05$ and $x = 0.6$. (b) Linear piecewise approximations for the same values of x.
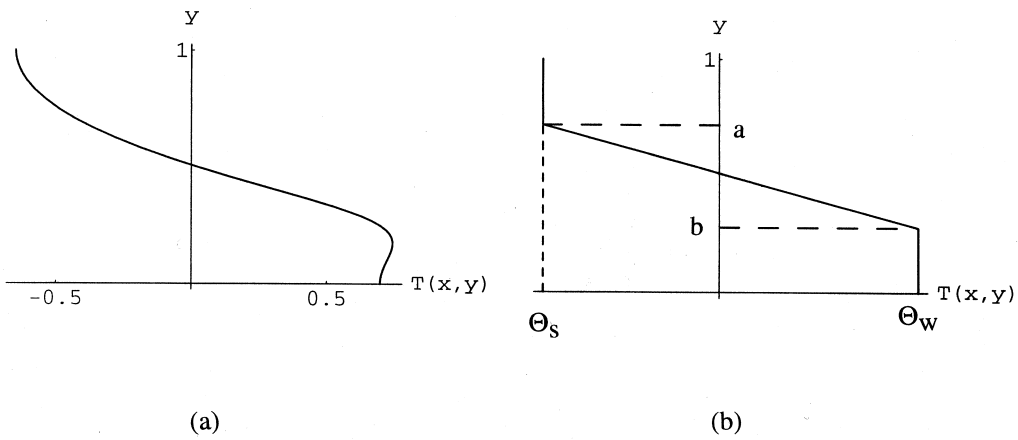

Fig. 10. Vertical temperature profiles when the bottom plate is insulating and $b = 0.25$. (a) Exact profile for $x = 0.2$. (b) Linear piecewise approximation.

$$p = \Theta_{\rm S}(x)[F_1(y) - h] + \Theta_{\rm W}(x)G_1(y) \qquad (23)$$

where $F_1(y)$ and $G_1(y)$ are integrals of respectively $F(y)$ and $G(y)$ that allow for continuity of the pressure at $y = a$ and $y = b$ and for the boundary condition: $p(h) = 0$. Substitution of the above expression in equation (21) yields

$$\partial_{yy}u = (Bo\, A - \Theta(x))\, \partial_x h + F_1(y)\, \partial_x\Theta_{\rm S} + G_1(y)\, \partial_x\Theta_{\rm W}.$$

After integrating twice the above equation and using successively the stress free condition $\partial_y u = 0$ at $y = h$,

and the boundary condition $u = 0$ at $y = 0$, one gets an expression for u that has not been reported here. Then, satisfaction of the flux conservation condition

$$\int_0^h u\,{\rm d}y = 0$$

leads to

$$\mu_1\, \partial_x\Theta_{\rm S} + \mu_2\, \partial_x\Theta_{\rm W} - (Bo\, A - \Theta_{\rm S})\frac{h^3}{3}\partial_x h = 0 \qquad (24)$$

where the expressions of the two coefficients μ_1 and μ_2 are given in the Appendix in terms of a, b and h. Since $h > a > b$, it can be shown that μ_1 and μ_2 are always positive. Moreover, μ_1 and μ_2 that behave like h^4 are rewritten $\mu_1 = h^4 \hat{\mu}_1$ and $\mu_2 = h^4 \hat{\mu}_2$. The new coefficients $\hat{\mu}_1$ and $\hat{\mu}_2$ now express in terms of the ratios a/h and b/h that will be approximated by their values for $h = 1$. It comes from equations (9) and (10) that $\partial_x \Theta_W = (1 + \lambda) \partial_x \Theta_S$ where λ is a function of the x variable, being equal to $\lambda(x) = \frac{1}{2}(1 + \cos \pi b)[\text{sh}(\pi x/2)]^{-2}$. The quantity λ diverges close to the wire location ($x \to 0$) and tends to zero for large values of x. To avoid divergence problems when integrating equation (24) we shall consider λ as a constant, its value being estimated at an intermediate value of $x < 1$. For instance, if $x = b = 1/4$ we get $\lambda = 5.25$. This leads to the relation between the deformation and the surface temperature distribution

$$h = \left(1 - \frac{\Theta_S}{Bo\, A}\right)^{-\mu} \tag{25}$$

where $\mu = 3[\hat{\mu}_1 + (1 + \lambda)\hat{\mu}_2]$ is positive. It is shown in the Appendix that the order of magnitude of the leading term in $\hat{\mu}_1$ is 0.12, while $\hat{\mu}_2$ is smaller and vanishes when $a = b = 0$. Provided that $\Theta/Bo\,A$ remains small to prevent h from going to infinity, this relation shows that the deformation above the wire corresponds to a bump ($h > 1$) contrary to what happens when thermocapillary effects are dominant.

The order of magnitude of the deformation has been estimated when the position of the wire is located at $b = 1/4$ from the bottom conducting boundary. Taking $a = 2b$, which corresponds to the vertical temperature profile depicted in Fig. 9, yields $\hat{\mu}_1 = 0.12$, $\hat{\mu}_2 = 8 \times 10^{-3}$ and consequently $\mu = 0.5$. From the experimental data of Ref. 4 we obtain that the variation range of $Bo\,A$ is between 10 and 50. Thus, applying formula (25) when $Bo\,A = 25$ leads to a deformation above the wire of the order $3 \times 10^{-3} d$, which is slightly larger than the deformation in the opposite direction due to purely thermocapillary effects (Section 4). This order of magnitude is compatible with the through-to-crest elevation differences Kayser and Berg [9] found in the range 0–100 μm.

6. Buoyant-thermocapillary flow

When thermocapillary and buoyancy effects are acting simultaneously, the velocity scale in equation (19) is kept equal to $U_S = Ma\,\kappa/L$ which is the same choice as in Section 4. Therefore, the factor in front of T in this equation is the ratio of the Rayleigh number to the Marangoni number and equation (20) is now replaced by

$$\partial_y p = \frac{Ra}{Ma} T(x, y)$$

which is solved by assuming for $T(x, y)$ the same decomposition as in equation (22) of Section 5. Thus, introducing the notation $W = Ra/Ma$, the pressure is deduced from expression (23) which has to be multiplied by W in the present case. Once p is known, equation (21) for u becomes

$$\partial_{yy} u = [Bo\, A - W\Theta_S(x)]\, \partial_x h$$
$$+ W[F_1(y)\, \partial_x \Theta_S + G_1(y)\, \partial_x \Theta_W]$$

that is solved with the boundary conditions

$$u(0) = 0, \quad \text{and } \partial_y u + \partial_x \Theta_S = 0, \quad \text{at } y = h.$$

The calculations which are very similar to those performed in the two previous sections have not been repeated here. Applying the flux conservation condition lead to the relation

$$h^2 = \frac{W_T}{W} + \left(1 - \frac{W_T}{W}\right)\left(1 - \frac{W\Theta}{Bo\, A}\right)^{-2\mu} \tag{26}$$

where we have introduced the notation $W_T = (3/2\mu)$. The parameter μ has the same meaning as in the previous section and thus W_T takes different values according to the position of the wire and the thermal condition on the bottom plate.

Considering that $(W/Bo\, A) = \alpha(Q/\kappa)$ is a small quantity, it will be used as an expansion parameter in the right-hand-side of equation (26). At the leading order, we get the result

$$h^2 = 1 - \frac{3\Theta}{Bo\, A}\left(1 - \frac{W}{W_T}\right). \tag{27}$$

Thus, $W > W_T$ implies that $h > 1$ while $W < W_T$ implies that $h < 1$. At $W = W_T$, the opposite actions of thermocapillarity and buoyancy tend to restore a flat interface. Moreover, expression (27) allows to recover the results obtained in the previous sections for the limiting cases $W = 0$ [equation (17)] and $W \gg 1$ [equation (25)].

7. Conclusions

We have developed a simple model to describe the flow induced by a hot wire located under the free surface of a liquid. Restriction to diffusive heat transport enabled us to solve separately for the temperature distribution and afterwards for the streamfunction and the deformation of the free surface. The temperature distribution was found by applying the method of images while considering the fluid at rest and a plane free surface. Then, the thin-layer approximation was used to derive the streamfunction and the position of the free surface. We have considered two different driving mechanisms for the liquid motion. In Section 4, where only thermocapillary effects are taken into account, it is found that the free

surface just above the wire deflects to a concave surface as it was also the case in Refs [6] and [7] that considered different heat sources. In Section 5, where buoyancy effects are responsible for fluid motion it is found that the free surface just above the wire deflects to a convex surface. A comparison ought to be made with what happens in fluid layers heated from below when Rayleigh–Bénard or Bénard–Marangoni instabilities arise. It is known that above onset, the convective cells arrange in an hexagonal planform with the interfacial shape above ascending flow being elevated or depressed whether the driving mechanism is thermocapillarity or buoyancy. We have shown that this conclusion remains true even when the initial thermal gradient has an horizontal component. The case where thermocapillarity and buoyancy are acting simultaneously is treated in Section 6. It is shown that the shape of the free surface depends on the ratio W of Marangoni number to Rayleigh number.

Our results agree with previous findings obtained by Kayser and Berg [9] when considering the interfacial shape of a liquid layer heated from below by a straight wire ($b = 0$). However, the mathematical model studied in Ref. [9] suffers some limitations. In particular, the rate of energy supply from the line source is modeled by a constant term in the thermal energy equation and represents a heat production uniformly distributed over the volume of liquid. Moreover, the heating rate used in their numerical calculations was very small to avoid problems of stability and convergence.

Another limitation that prevents the use of full numerical simulations for thermally driven flows are the difficulties to resolve the small length scales, which explains the growing interest for theoretical models to understand the dynamics of the flow in corner regions [16]. Until now, numerical simulations of thermocapillary flows have been performed for values of the Prandtl number barely exceeding $Pr = 7$ in extended geometry [17] and $Pr = 100$ in a square cavity [16]. Moreover, a closed-form solution for the primary flow is sometimes a good starting point for analyzing its stability toward three dimensional disturbances as it has been done by Vrane and Smith [18] for an annular geometry. When solving for the disturbances and after having neglected inertial and convective terms, these authors only found steady solutions. In the set of experiments performed with a long wire [3, 4], the primary flow always becomes unstable toward traveling waves propagating in the direction of the wire. This behavior is different from what has been observed when the flow is driven by a pure horizontal thermal gradient [19]. In this latter case and depending on the height of fluid, the unstable patterns are either stationary longitudinal rolls or oblique waves propagating in a direction nearly perpendicular to that of the thermal gradient. A model based on a plane flow approximation has been able to reproduce these two typical behaviors [20]. In presence of a wire, the primary flow is two-dimensional and interfacial deformations above the wire are detected in the experiments through shadowgraphic pictures but the magnitude of these deformations along the *x*-direction has not yet been measured. It is only above the threshold for instability that the amplitude of the deformations along the *y*-direction is known.

We suspect that the interfacial deformations associated to the primary flow may influence the spatio-temporal behaviors of the unstable modes. However, more experimental results are needed, in particular to confirm our predictions as to the shape of the interface above the wire when either surface tension effects or buoyancy effects are driving the flow. The thin layer approximation is also questionable, being more or less satisfied according to the position of the wire and the thermal condition on the bottom plate. Since the Reynolds number is small in the experimental conditions of Ref. [3] a forthcoming improvement of our model will be to relax the additional simplification $A \to 0$ and to use Stokes approximation to derive a solution for the thermally driven flow.

Appendix

The coefficients μ_1 and μ_2 result from the flux conservation condition. They appear as the sum of three contributions respectively proportional to $(h-a)$, $\delta = a-b$ and b:

$$\mu_1 = \frac{h-a}{8}\left\{(h^2-a^2)(h+a)+\frac{\delta}{3}(b^2+2ab+3a^2)\right\}$$

$$+\frac{\delta}{12}\left\{h[3(h-a)(a+b)+\delta(a+2b)]+\frac{\delta^3}{10}\right\}$$

$$+\frac{b^2}{12}[2h(h-b)+h^2-a^2].$$

The above expression reduces to $\mu_1 = (h^4/8)$ when $a = b = 0$, which corresponds to a flat vertical temperature profile valid away from the wire when the bottom boundary is insulating. When the bottom boundary is conducting and $a = b = 1/4$, μ_1 takes the value $0.1225h^4$.

In the case of a conducting bottom boundary:

$$\mu_2 = \frac{a}{24}(h-a)[a^2+ab+b^2]$$

$$+\frac{\delta}{120}(4a^3+8a^2b+2ab^2+b^3)$$

$$+\frac{b^2}{120}(b^2+10a^2).$$

When $a = b = 1/4$, the above coefficient takes the particular value $\mu_2 = 1.8 \times 10^{-3}$.

In the case of an insulating bottom boundary:

$$\mu_2 = \frac{1}{24}(h-a)(a^3 + a^2b + ab^2 + b^3)$$

$$+ \frac{\delta}{30}\left(a^3 + 2a^2b + \frac{1}{2}ab^2 + \frac{3}{2}b^3\right) + \frac{b^2}{120}(6b^2 + 5a\delta).$$

Acknowledgements

References

[1] M.E. Weill, M. Rhazi, G. Gouesbet, Experimental investigation of oscillatory phenomena produced by a hot wire located near and below a free surface, Journal de Physique 46 (1985) 1501–1506.

[2] C. Roze, Etude des oscillations créées par un fil chaud placé juste au-dessous de la surface d'un liquide, Thèse de doctorat de l'Université de Rouen, France, 1989.

[3] J.M. Vince, M. Dubois, Hot wire below the free surface of a liquid: structural and dynamical properties of a secondary instability, Europhysics Letters 20 (1992) 505–510.

[4] J.M. Vince, Ondes propagatives dans des systèmes convectifs soumis à des effets de tension superficielle, Thèse de doctorat de l'Université Paris VII, France, 1994.

[5] C.-S Yih, Fluid Mechanics, McGraw-Hill, 1969, p. 412.

[6] S.M. Pimputkar, S. Ostrach, Transient thermocapillary flow in thin liquid layers, Physics of Fluids 23 (1980) 1281–1285.

[7] D.L. Hitt, M.K. Smith, Radiation driven thermocapillary flows in optically thick liquid films, Physics of Fluids A 5 (1993) 2624–2632.

[8] J. Burgete, H.L. Mancini, C. Pérez-Garcia, Dynamics of a secondary instability in Bénard–Marangoni convection with unidimensional heating, Europhysics Letters 23 (1993) 401–407.

[9] W. Kayser, J. Berg, Surface relief accompanying convection in liquid pools heated from below, Journal of Fluid Mechanics 57 (1973) 739–752.

[10] A. Thess, D. Spirn, B. Jüttner, A two-dimensional model for slow convection at infinite Marangoni number, Journal of Fluid Mechanics 331 (1997) 283–312.

[11] K.M. Yu, M.W. Nansteel, Buoyancy-induced Stokes flow in a wedge-shaped enclosure, Journal of Fluid Mechanics 221 (1990) 437–451.

[12] M. Jakob, Heat Transfer, vol. I, John Wiley, New York, 1964, p. 322.

[13] H. Lamb, Hydrodynamics, 6th ed., Cambridge University Press, Cambridge, 1932, p. 227.

[14] H. Mekias, J.M. Vanden-Broeck, Subcritical flow with a stagnation point due to a source beneath a free surface, Physics of Fluids A 3 (1991) 2652–2658.

[15] J.A. Whitehead, M.M. Chen, Thermal instability and convection of a thin fluid layer bounded by a stably stratified region, Journal of Fluid Mechanics 40 (1970) 549–576.

[16] D. Canright, Thermocapillary flow near a cold wall, Physics of Fluids 6 (1994) 1415–1424.

[17] L.J. Peltier, S. Biringen, Time-dependent thermocapillary convection in rectangular cavity: Numerical results for a moderate Prandtl number fluid, Journal of Fluid Mechanics 257 (1993) 339–357.

[18] D.R. Vrane, M.K. Smith, The influence of domain curvature on the stability of viscously-dominated thermocapillary flows, in: Y. Renardy, A. Coward, D. Papageorgiou, S.M. Sun (Eds.), Advances in Multi-Fluid Flows, SIAM Philadelphia, 1996, pp. 219–238.

[19] F. Daviaud, J.M. Vince, Traveling waves in a fluid layer subjected to a horizontal temperature gradient, Physical Review E 48 (1993) 4432–4436.

[20] J.-F. Mercier, C. Normand, Buoyant-thermocapillary instabilities of differentially heated liquid layers, Physics of Fluids 8 (1996) 1433–1445.